Size Selected Clusters on Surfaces

2013 J. Phys.: Conf. Ser. 438 012005

(http://iopscience.iop.org/1742-6596/438/1/012005)

Journal of Physics: Conference Series **438** (2013) 012005 doi:10.1088/1742-6596/438/1/012005

Size Selected Clusters on Surfaces

X. Tang, X. Li, Y. Wang, K. Wepasnick, A. Lim, D. H. Fairbrother, K. H. Bowen[1],

Departments of Chemistry and Materials Science, Johns Hopkins University, Baltimore, MD USA

T. Mangler, S. Noessner, C. Wolke, M. Grossmann, A. Koop, G. Gantefoer

Department of Physics, University of Konstanz, Konstanz, Germany

B. Kiran

Departments of Chemistry and Physics, McNeese University, Lake Charles, LA, USA

A. K. Kandalam

Deptartment of Physics, West Chester University, West Chester, PA

[1] E-mail : kbowen@jhu.edu

Abstract. Size selected metal oxide, sulfide and oxynitride clusters, soft-landed onto highly ordered pyrolytic graphite (HOPG) at room temperature, have been studied in this work. Based on their size and chemical compositions, the deposited clusters have exhibited various surface structures as illustrated by *in situ* Scanning Tunnelling Microscope (STM) and *ex situ* Atomic Force Microscope (AFM). In contrast to pure metal clusters, size selected metal compound clusters have shown different surface behaviours due to their different cluster-surface interactions.

1. Introduction

Clusters contain an ensemble of bound atoms whose size is intermediate between an individual molecule and a bulk solid. As such, clusters are a unique class of material which continues to attract intense scientific interest due to the fact that they often exhibit extraordinary electronic, optical, catalytic properties, etc. [1-3] Many of these properties are strongly size-dependent, e.g. gold clusters in the size regime of 2-4 nm catalyze CO oxidization at low temperatures, whereas bulk gold is catalytically inert [4]. Metal oxides have also been shown to exhibit size-dependent reactivity. For example, in a study by Castleman *et al*. [5], the reactivity of group V transition metal oxide cluster cations with *n*-butane has been shown to be strongly dependent on the number of metal atoms in the cluster. This underscores the need for means that allow one to control the size of deposited clusters as a way of tailoring the properties and functions of these nanostructures. Amongst the various methods of cluster deposition, which include conventional molecular beam [6] and wet-chemistry [7] techniques, the soft-landing of size selected gas phase clusters onto supported surfaces is a promising

[1] To whom any correspondence should be addressed.

approach due to its ability to utilize gas phase clusters that occur in a wide range of sizes and chemical compositions. However, controlling the ultimate size, structure, and therefore functionality of deposited clusters created by this means relies on understanding the relationships between the size of the incident gas phase clusters and the nature of the deposited clusters, determined by cluster-cluster and cluster-surface interactions [8; 9].

Our knowledge of the structures that gas phase clusters adopt on solid surfaces comes predominantly from studies on metal clusters deposited by soft-landing, or, in a few cases, low energy ion beam deposition on atomically smooth surfaces such as highly ordered pyrolytic graphite (HOPG) and mica [10-17]. In general, the surface structures formed have been found to depend on the size of the incident gas phase clusters. For example, antimony clusters deposited on graphite surface coalesce into larger clusters when the incident cluster size is small (Sb_4). In contrast, cluster-cluster interactions become less favorable when larger incident antimony clusters (Sb_{350}, Sb_{2200}) are deposited [11]. These size-dependent effects are ascribed to the lower surface mobility of larger clusters, coupled with their greater thermodynamic stability due to the lower fraction of surface atoms. The observations are, in turn, consistent with experiments on gold clusters. In a series of experiments, small gold clusters (Au_1, Au_3, Au_7) were observed to be mobile on HOPG before coalescing into larger clusters with a much larger diameter [18], while large gold clusters (Au_{250}) were less mobile and only partially coalesced into fractal structures [19]. However, in experiments performed using size selected silver clusters, it was observed that silver clusters containing 50 to 250 atoms deposited onto HOPG diffuse and coalesce into larger nanoparticles with a diameter of about 14 nm, irrespective of the incident gas phase cluster size [13]. In contrast, our knowledge of the size-dependent surface behavior of metal compound clusters (e.g, metal oxides[20-22], sulfides[23], nitrides), is extremely limited despite their importance in catalysis and material science [24].

From these discussions, understanding how the size of incident metal compound clusters affects their surface structures and properties is clearly important. In this proceeding, we have focused on three different types of clusters: molybdenum oxides, lead sulfides, and titanium oxynitrides. Results obtained by local probe microscopes reveal that these metal compounds sometimes result in significantly different surface structures from their pure metal clusters. We attribute these differences to their different cluster-cluster and cluster-surface interactions.

2. Apparatus

Cluster anions were produced by the cluster deposition apparatus shown in Figure 1. Briefly, a metal target was placed in a cylindrical magnetic field and biased to -500 V. A mixture of argon and helium was then introduced into the source. Argon ions created within the source sputtered the metal target, producing metal clusters. To produce different types of clusters, different reactive gases were introduced to react with the metal cluster vapors: Oxygen (O_2) was used to produce oxide clusters; metal sulfides were prepared by reacting metal ions with hydrogen sulfide (H_2S); finally, for titanium oxynitride clusters, nitrogen was provided by ammonia gas (NH_3), and oxygen came from residual gases such as water (H_2O). The added helium served to cool and transport the ions downstream.

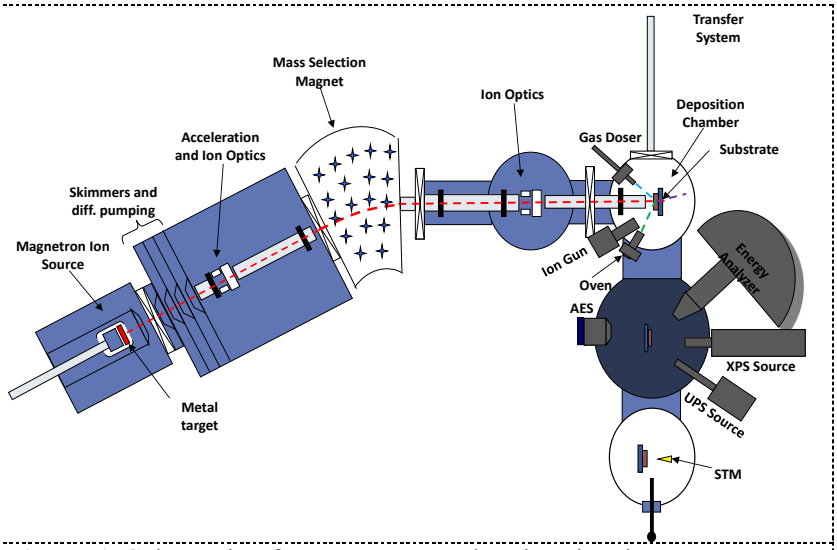

Figure 1. Schematic of our apparatus, showing the cluster deposition, beam-line, and the surface analytical instrumentation.

After the clusters anions were produced, they were accelerated before entering a magnetic sector mass spectrometer (25◦ sector magnet with resolution of m/Δm= 20). By tuning the magnetic field strength and/or the ion energy, clusters of various sizes were mass-selected and then passed through a series of ion optics before entering a Ultra-High Vacuum (UHV) deposition chamber where they were soft-landed (kinetic energy < 0.1eV/atom) onto a 1 cm^2 piece of freshly peeled HOPG.

Once clusters had been deposited onto the HOPG substrate, samples could be internally transferred to the adjunct UHV chamber, where they could be characterized by *in situ* Auger electron spectroscopy (AES), X-ray Photoelectron Spectroscopy (XPS), and Scanning Tunneling Microscopy (STM). *Ex situ* Atomic force microscopy (AFM) was also employed to characterize the structures of deposited clusters.

3. Structures of Size Selected of Clusters on Surfaces

3.1. Metal /Metal Oxide Clusters on HOPG

The mobility and aggregation behaviors of metal versus metal oxide clusters on HOPG surfaces have been examined as a function of their coverage. To accomplish this, mass-selected, cluster anion beams of Mo_{100}^- and $(MoO_3)_{67}^-$ were produced in a magnetron sputter source and soft-landed onto HOPG under UHV conditions. These two clusters were chosen because they possess essentially the same masses and consequently could be soft-landed with the same low kinetic energies, resulting in deposition energies of ~0.1 eV/ atom. The *in situ* AES confirmed the chemical composition of molybdenum metal and metal oxide clusters, respectively. Their surface morphologies were then characterized as a function of cluster coverage by using *in situ* STM and *ex situ* AFM. Both STM and AFM results indicated high mobility for the metal atom clusters on HOPG at room temperature as shown Figure 2(a) and Figure 3.

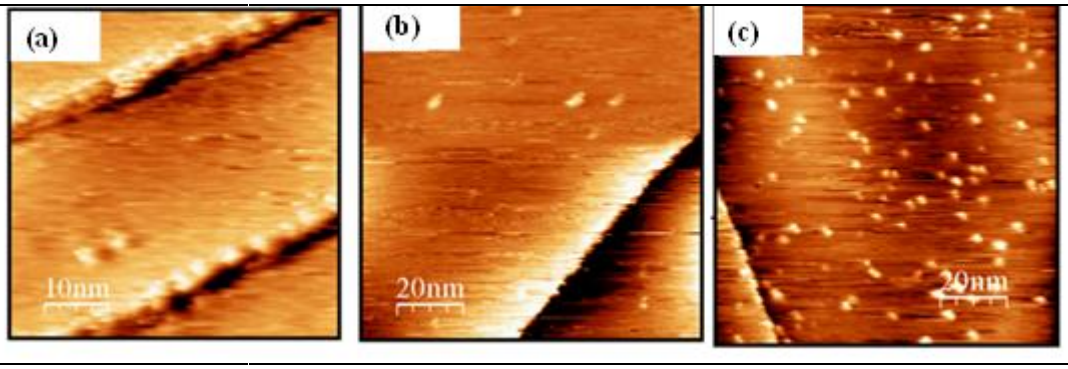

Figure 2. Deposited (a) Mo_{100} clusters and (b)(c) $(MoO_3)_{67}$ clusters on HOPG imaged by *in situ* STM .

At low coverages, Mo_{100} clusters migrated over the surface and nucleated preferentially at step edges as shown in Figure 2(a) and Figure 3(a), but at higher coverages they aggregated on the terraces until a fully saturated over-layer was eventually created, as shown in Figure 3(b). This behavior by metal clusters on HOPG surfaces was in accordance with prior studies on other metal cluster systems due to the high mobility of metal clusters on HOPG substrates.[10] With the same low kinetic energies and the same masses, one might have expected the metal oxide clusters to disperse over HOPG in the same way. In contrast with Mo_{100} metal clusters, the $(MoO_3)_{67}$ oxide clusters, instead of showing high mobility, produced a random array of adsorbed clusters at all coverages as shown in Figure 2(b)(c) . Consequently, on the same type of surface and with the same energy per atom, these metal oxide clusters were comparatively immobile relative to metal clusters, and differences in the mobility and aggregation behaviors of Mo_{100} and $(MoO_3)_{67}$ clusters at room temperature were attributed to differences in the interactions of metal and metal oxide clusters with carbonaceous surfaces.

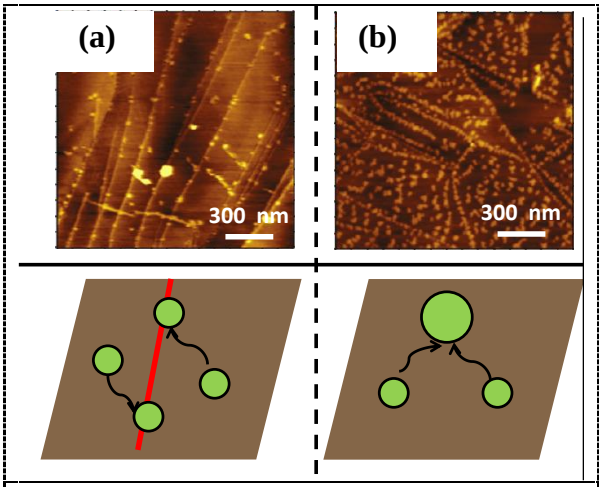

Figure 3 Deposited Mo_{100} clusters on HOPG imaged by *ex situ* AFM: (a) low coverage (b) high coverage

3.2. Lead Sulfide: Its Clusters and its Embryonic Crystal

It has been a goal of cluster science to connect the microscopic, molecular level world to the macroscopic, bulk level world.[1] In particular, at what size do clusters (aggregates) first take on properties which are characteristic of the bulk? Here, we are interested in identifying the smallest, viable crystalline unit of the lead sulfide rock salt crystal, i.e., its “baby crystal."[23]

To set the stage for the STM studies of "baby crystals," our previous work combined both experiments and theory to explore the geometric structures and electron affinities of small, gas-phase, lead sulfide clusters, $(PbS)_n$, ranging in size from n = 2-15. [25]

First, photoelectron spectroscopy was conducted on size-selected cluster anions to acquire both ground and excited state electronic structure information as well as the electron affinity values of the cluster anions' neutral counterparts. Figure 4 and Figure 5 display the calculated geometric structures of neutral and anionic $(PbS)_n$ clusters with n=1-10, respectively. Further comparison of the calculated electron affinities and vertical detachment energies with measured photoelectron spectra has authenticated the calculated structures. Among these calculated structures, the $(PbS)_4$ cube was found to be the most stable of the lead sulfide clusters studied due to a large, calculated HOMO-LUMO gap (2.96 eV), and it was also suggested to be the preferred product of cluster fragmentation processes. These findings are consistent with the fact that the primitive cell in crystalline lead sulfide is made up of four lead sulfide molecules. Notably, a structural growth pattern for the lowest energy isomers in this cluster size range has been proposed here based on a two-dimensional stacking of face-sharing (side-by-side) lead sulfide cubical units. For example, the face sharing of $(PbS)_4$ cube would lead to the lowest energy isomer of $(PbS)_8$. However, over the studied size range, the lead and sulfur atoms in these structures possessed a maximum of five-fold coordination, rather than the six-fold coordination found in bulk, lead sulfide crystals. As a general conclusion for these calculated structures, lead sulfide clusters in this size range form slightly distorted, fused cuboids.

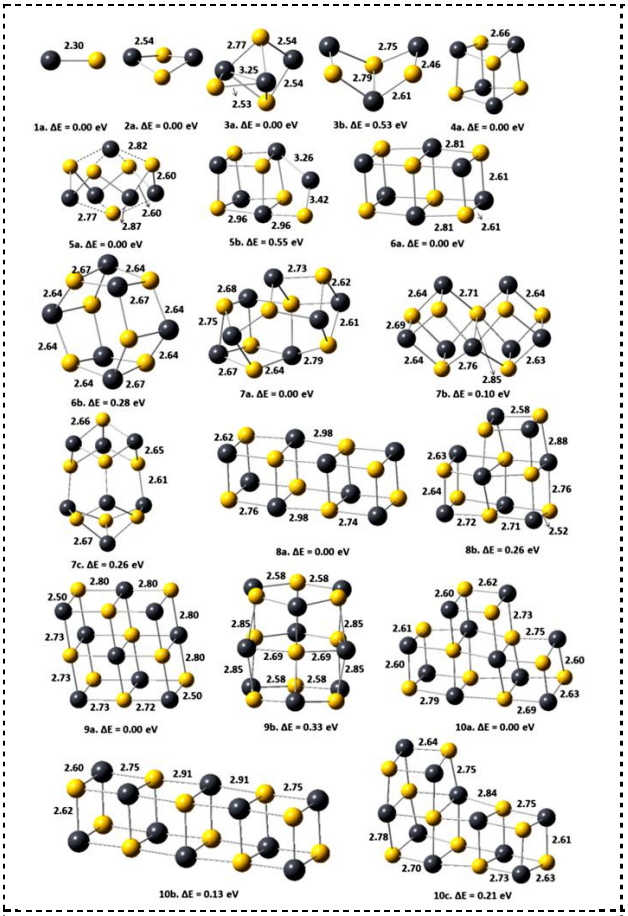

Figure 4. The lowest energy and higher energy isomers of neutral $(PbS)_n$ (n = 1–10) clusters.

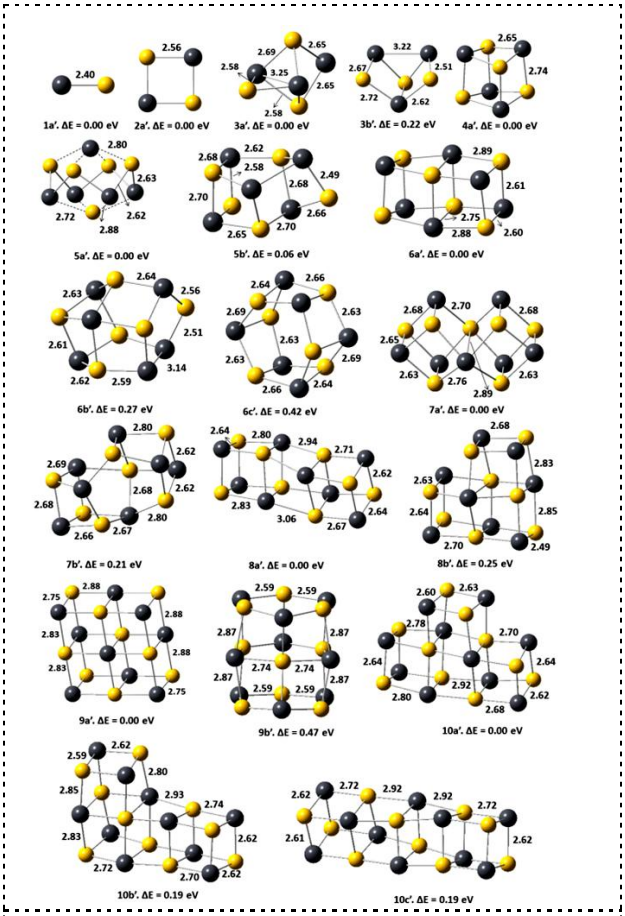

Figure 5. The lowest energy and higher energy isomers of anionic $(PbS)_n$ (n = 1–10) clusters.

Since lead sulfide clusters in this size range were too small to adopt bulk-like six-fold coordination, this left open the question: what is the smallest $(PbS)_n$ cluster size that can do so and that can also be

replicated to form the bulk crystalline material? The successive dimerization processes from the $(PbS)_4$ cluster were used to search for this minimum cluster size, as illustrated in Figure 6. The dimerization leads to the formation of $(PbS)_n$ clusters from n=4 to 8, 16, and further on until 32, where the inner $(PbS)_4$ core of $(PbS)_{32}$ enjoys bulk-like six-fold coordination. On other hand, the calculated structures of $(PbS)_n$ cluster with n=12, 20, 24 did not have six-fold coordination in their bulk. According to the calculations, the lowest energy isomer of $(PbS)_{28}$ did have bulk-like six-fold coordination. However, the replication of $(PbS)_{28}$ failed to lead to the bulk rock-salt structure while $(PbS)_{32}$ did. Thus, cubic $(PbS)_{32}$ is a "*baby crystal*," i.e., the smallest cluster exhibiting six-fold coordination that can be replicated to obtain the bulk crystal. Additionally, the calculated dimensions of the $(PbS)_{32}$ cluster further provide a rubric for understanding how the successive fusion of multiple $(PbS)_{32}$ building blocks results in the formation of square and rectangular, crystalline nano-blocks, e.g., $(PbS)_{64}$, $(PbS)_{128}$, and $(PbS)_{256}$, with specific dimensions as shown in Figure 7.

We then conducted cluster deposition to test the above theoretical predictions. Herein. mass-selected $(PbS)_{32}$ clusters were soft-landed onto HOPG surfaces and imaged by STM to gauge their dimensions. These dimensions were then compared with those of the fused $(PbS)_{32}$ nano-blocks predicted by theory.

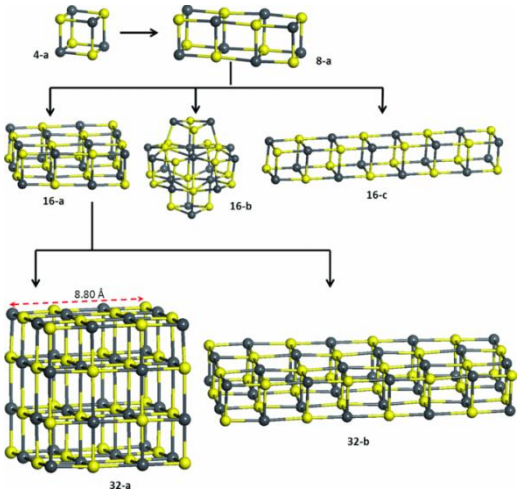

Figure 6. The growth pattern of lead sulfide cluster structures via dimerization of $(PbS)_{4n}$ units. For $(PbS)_{16}$ and $(PbS)_{32}$, both, the lowest, (a), and higher, ((b) and (c)), energy isomers are shown.

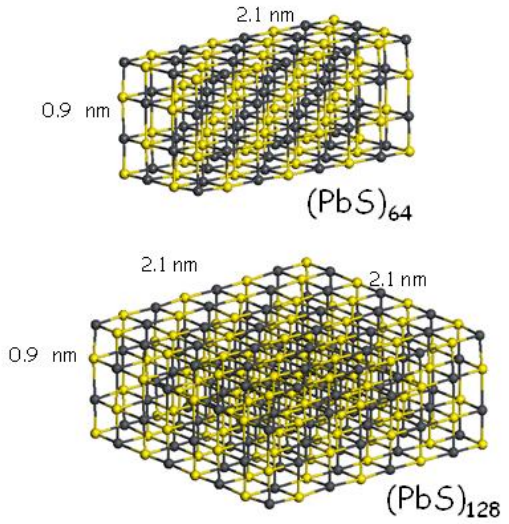

Figure 7. Calculated lowest energy structures for the $(PbS)_{64}$ and $(PbS)_{128}$ nano-blocks.

The chemical compositions of lead sulfide clusters were confirmed by *in situ* XPS measurements. The XP spectra of Pb (4f) and S (2p) regions are presented in Figure 8. Both the peak transitions of $Pb(4f_{7/2})$ centered at 137.4 eV and S(2p) centered at 160.6 eV indicated the unoxidized nature of the deposited lead sulfide clusters.[26] A further quantitative analysis of XPS results revealed that the ratio of Pb to S was found to be about 1:1, which doubly confirmed the deposition of PbS clusters.

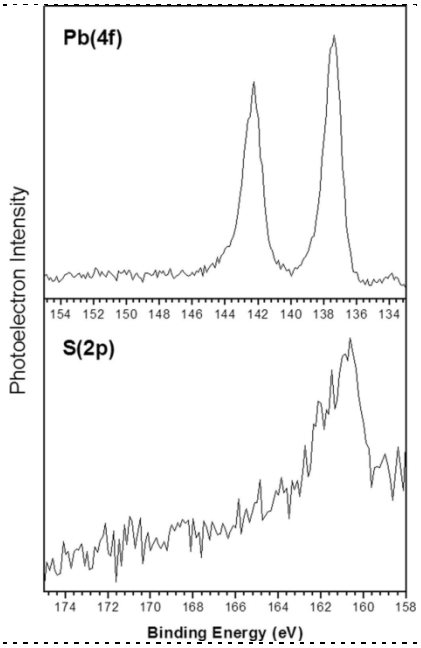

Figure 8. X-ray photoelectron spectra [Pb(4f) and S(2p) regions] of lead sulfide aggregates on HOPG.

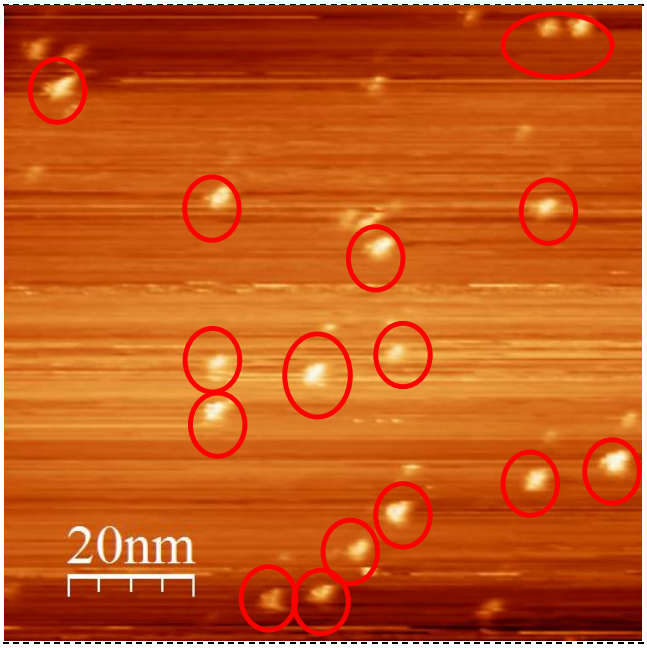

Figure 9. $(PbS)_{32}$ clusters deposited on HOPG by *in situ* STM

Given the presence of size-defined $(PbS)_{32}$ clusters on the surface as the starting point, we were assured that the observed STM images were the result of two-dimensional nucleation between $(PbS)_{32}$ clusters and/or between nano-blocks composed of multiple $(PbS)_{32}$ units. A typical STM image of the as deposited $(PbS)_{32}$ clusters at low coverage were displayed in Figure 9, in which many of these clusters exhibited non-spherical shapes, consistent with structures formed by the growth of cuboids. Two additional figures in Figure 10 are presented showing another two cluster that $(PbS)_{32}$ clusters have been deposited at low coverage. One of these figures shows an image of a square nano-block, while the other shows an image of a rectangular nano-block. Note that none of the clusters in the STM image have the dimensions of the originally deposited $(PbS)_{32}$ clusters; instead, they are significantly larger. This is because small $(PbS)_{32}$ clusters are mobile on HOPG; thus, they have aggregated into larger objects. Beyond qualitative assessments of shapes, STM imaging was also used to determine approximate lateral and vertical dimensions of the various aggregated clusters on the surface. We have observed STM images of these clusters, where the lateral dimensions are consistent with the predictions of theory. For example, the one labeled A has measured lateral dimensions, ~2 nm × ~2 nm corresponding to $(PbS)_{128}$. Likewise, the one labeled B has measured lateral dimensions,~4 nm × ~2 nm corresponding to $(PbS)_{256}$. Moreover, line-scans of adjacent nano-blocks, (e.g. $(PbS)_{128}$ and $(PbS)_{256}$) showed that both aggregates had heights in the range of 0.8 – 1 nm, consistent with the theoretical prediction of 0.88 nm for the heights of nano-blocks formed by the side-by-side aggregation of $(PbS)_{32}$ units. A further height analysis for a larger population of clusters was conducted to analyse the size distribution of the clusters. Consistent with the previous results, the height distribution of these clusters ranged from 0.8 to 1.2 nm, resulting from the two dimensional aggregation behaviours of $(PbS)_{32}$ clusters.

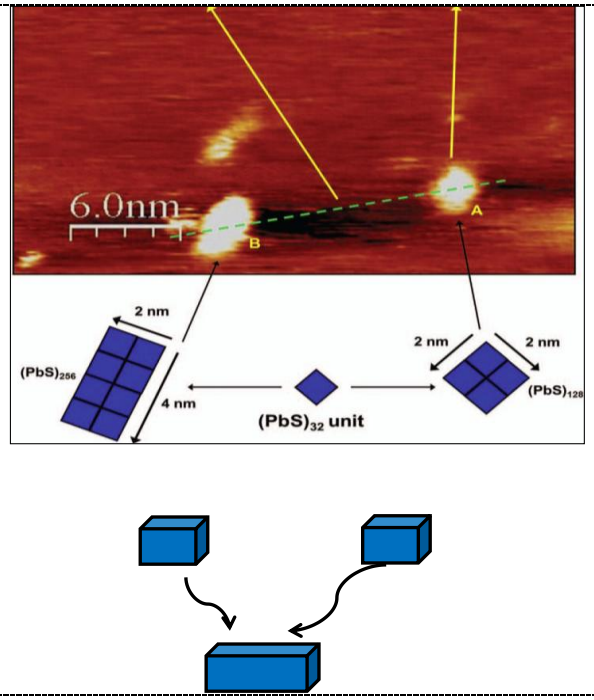

Figure 10. A STM image showing aggregates resulting from the soft-landing of mass-selected $(PbS)_{32}$ clusters onto a HOPG surface.

Therefore our STM images show shapes and dimensions that are consistent with the predictions of the theoretical part of this study. Thus, this study has provided a pathway for better understanding the mechanisms involved in the formation of this class of solids.

3.3. Titanium Oxynitride Snowflakes (Fractals)

It is known that titanium nitride clusters, $(TiN)_n$, can be prepared by ablating or sputtering titanium metal in the presence of NH_3 or N_2 gas[27; 28]. In our work, we magnetron sputtered titanium metal in the presence of ammonia and then size-selected and soft-landed $(TiN)_{141}$ onto HOPG. While still at 10^{-9} Torr, *in situ* XPS spectra of the deposited clusters was recorded to verify the chemical compositions of the as-deposited clusters.

Figure 11(a) showed the presence of XPS peak features in both the Ti (2p) and N (1s) regions, with an addition peak feature in O (1s) region that suggested the presence of oxygen within the clusters. While this was unwelcome, titanium (an excellent getter) had incorporated any available oxygen into the putative titanium nitride clusters.

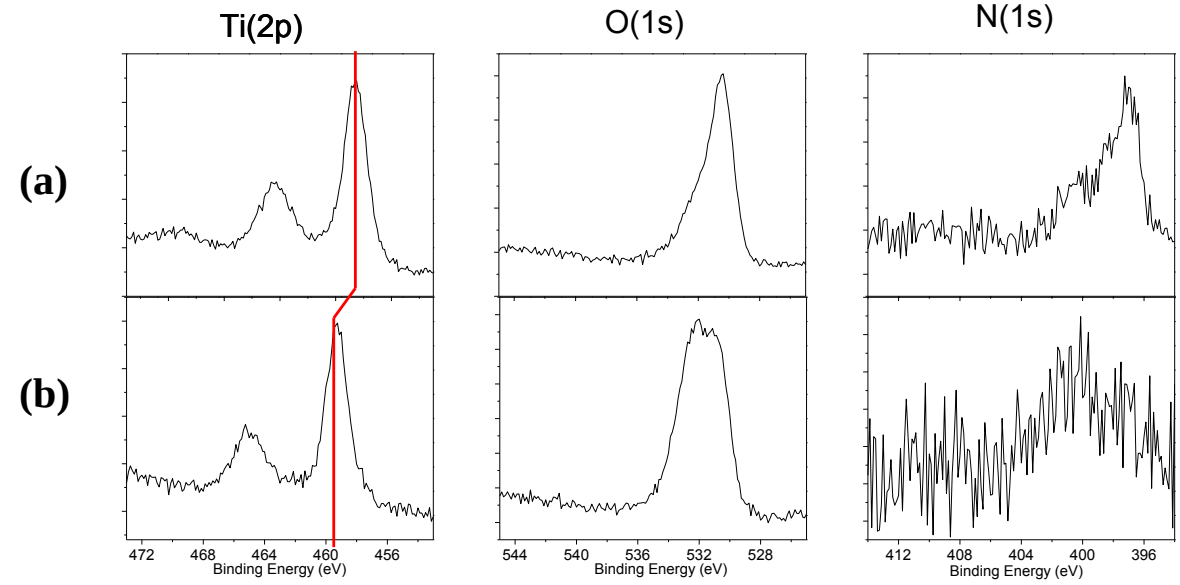

Figure 11. X-ray photoelectron spectra [Ti(2p) ,O(1s) and N(1s) regions] of (a) as-deposited and (b) air-exposed titanium oxynitride cluster aggregates on HOPG

While the sample was clearly contaminated by oxygen, thus making the as-deposited clusters essentially titanium oxynitride clusters instead of titanium nitride clusters, the clusters' surface structures were further characterized by *ex situ* AFM. This procedure necessitated exposing the sample to air. To our surprise, the resulting image in Figure 12 showed beautiful fractal (snowflake) patterns. The successive XPS characterization as shown Figure 11(b) showed the evidence for titanium and oxygen as expected, but much less nitrogen for the air-exposed clusters.

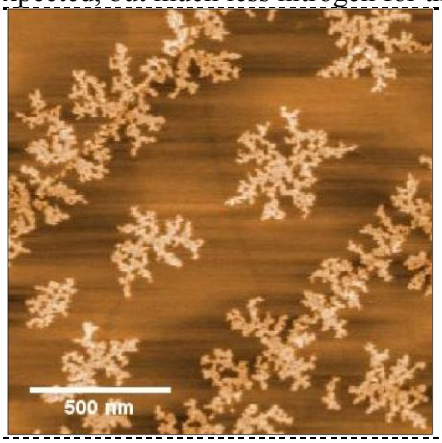

Figure 12. Fractal structures formed by deposited titanium oxynitride clusters

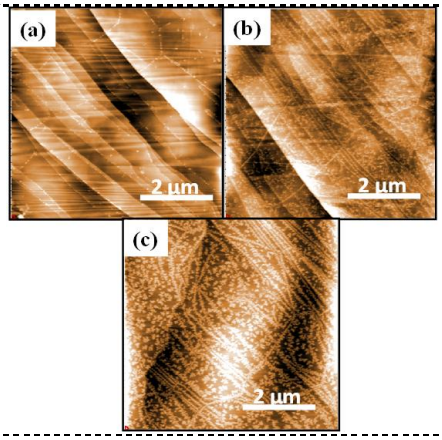

Figure 13. Deposited titanium oxide clusters by ex-situ AFM with coverage increasing from (a) to (c)

To study the effect of nitrogen on the structures, pure titanium oxide clusters with the same mass were produced by magnetron sputtering titanium metal with pure O_2 gas and with no NH_3 or N_2 gas. As expected, XPS confirmed that the cluster sample consisted only of titanium and oxygen. Then, the sample was exposed to air and recorded with *ex situ* AFM. No snowflakes had appeared for aggregated titanium dioxide clusters at low and medium coverages(Figure 13(a) and Figure 13(b), respectively). At much higher coverage, which corresponds to Figure 13(c), very small fractal structures begin to appear on the surface, indicating that, indeed, the presence of nitrogen had mattered.

The coverage of the titanium oxynitride clusters was varied systematically to investigate the formation of the fractal structures. The AFM images are shown in Figure 14, where coverage increases from (a) through (f). At the lowest coverage, nucleation along step edges is evident. As coverage increases, one observes randomly distributed aggregates on the terraces, which serve as feeds to further formation of fractal patterns. At the highest coverage, snowflakes are seen to form and to arrange themselves into intricate, elaborate patterns. Fractal patterns due to aggregation of atoms/molecules on surfaces have often been seen in the past, but only rarely due to mass-selected cluster deposition [10; 29; 30] and, to our knowledge, never under these circumstances. Usually, a diffusion-limited aggregation mechanism[31] is used to understand the growth behavior of the fractal structures. Within the growth model, the fractal formation is strongly correlated to the flux intensity of the incoming clusters from the gas phase. For low coverage, due to low flux intensity, there are not enough cluster-cluster interactions to immobilize the clusters on the terrace. Consequently, they diffuse on the terrace until they are trapped by the step edges. In contrast, as coverage increases, more cluster-cluster interactions are favored due to higher flux intensity. The abundance of cluster-cluster aggregations will then lead to the formation of nucleation seeds on the terrace as starting points for further fractal formations on the HOPG surface.

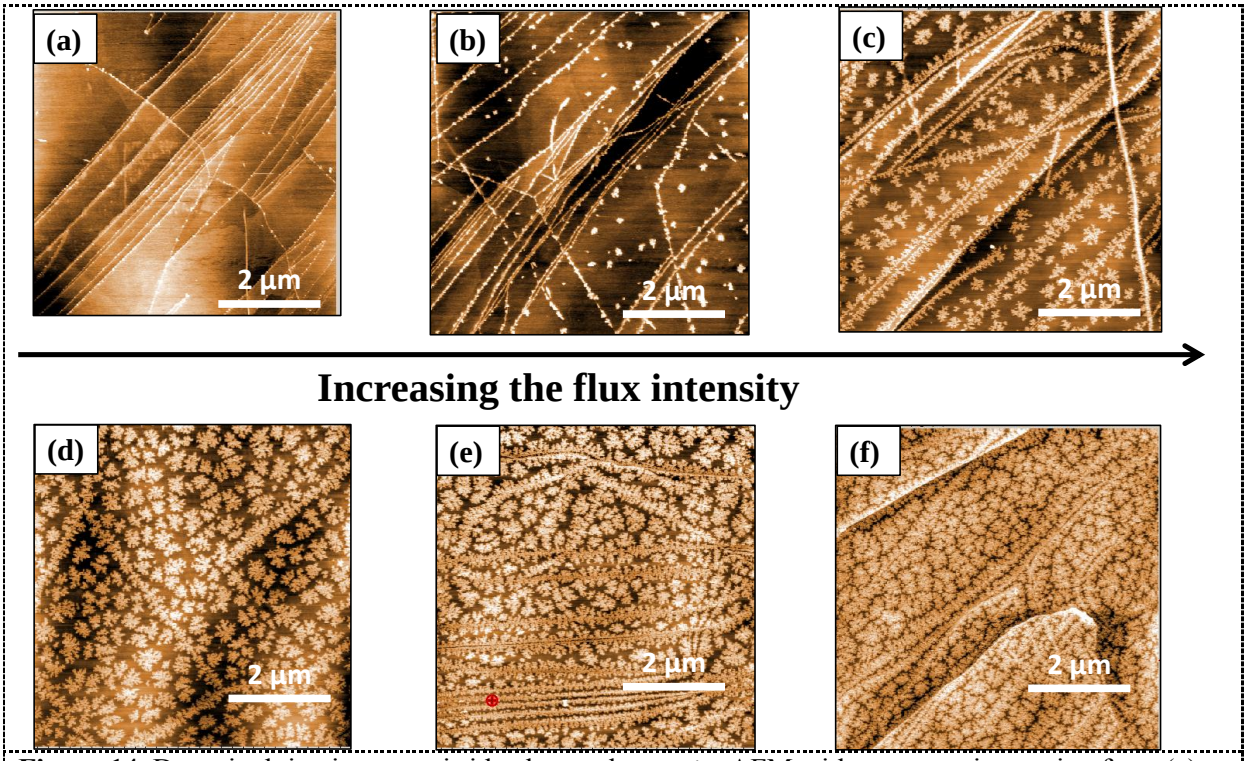

Figure 14. Deposited titanium oxynitride clusters by *ex situ* AFM with coverage increasing from (a) to (f)

A size-dependent study was also conducted by depositing the titanium oxynitride clusters with a different mass (3,700 amu) as presented in Figure 15(b). Compared to the same cluster with a higher mass (8,600 amu), the structures of clusters with lower mass showed much smaller and more compact fractal structures compared to Figure 15(a). The differences in structures of two clusters can be understood by an edge diffusion mechanism[32]; that is, clusters with a lower mass possess more active edge diffusion due to their higher mobility. Thus, once they are attached to the fractal island, they are more robust to diffuse along the edge in order to search for the adsorption sites corresponding to the global energy minimum. As a result, the deposition of smaller clusters will lead to more compact fractal patterns.

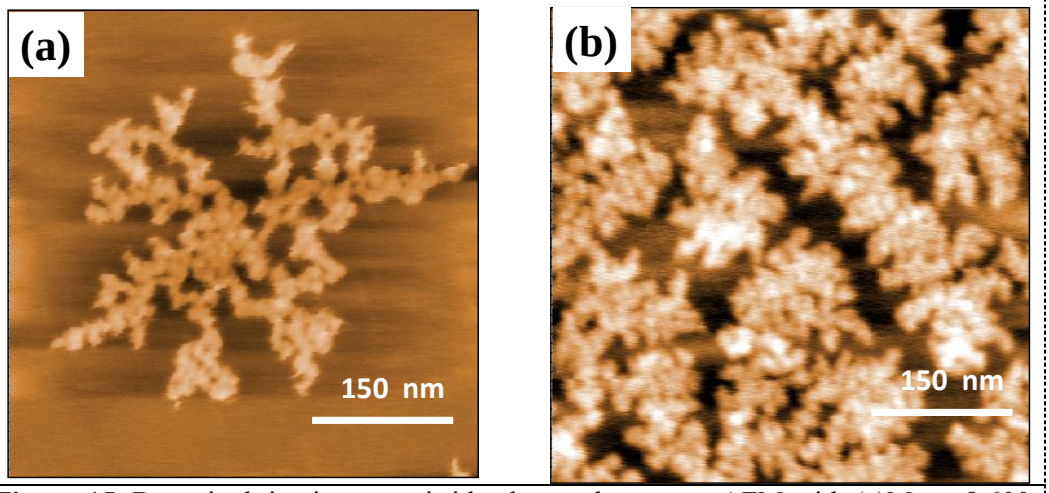

Figure 15. Deposited titanium oxynitride clusters by *ex situ* AFM with (a)Mass~8,600 amu and (b)Mass~3,700 amu

Herein, we have obtained fractal structures through the deposition of size-selected titanium oxynitride clusters on an HOPG surface. The nitrogen content was found to be responsible for the formation of fractal structures. Varying the flux intensity revealed the different stages of fractal growth. Furthermore, the fractal structures showed a strong size-dependent behavior, which provide possible pathways to regulating the fractal structure via size control.

4. Conclusion and Outlook

Three different types of systems of size-selected metal compound clusters were introduced in this proceeding. In all three systems, cluster behaviours significantly different from previously studied metal cluster systems were observed. Results from these studies illustrate how the surface morphologies of adsorbed clusters are influenced by their chemical composition, their size, and their coverage for metal compound clusters. The knowledge acquired here will benefit further applications of these metal compound clusters. For example, all three systems in this work have potential catalytic applications, i.e. molybdenum oxides are widely used in oxidative dehydrogenation, and lead sulfide is a good photocatalyst due its tunable band gap to adsorb solar light. Thus, these supported size-selected metal compound clusters may offer a new pathway to study their catalytic properties correlated to their size, structures, and chemical compositions.

Acknowledgments

This material is based upon work supported by the Division of Materials Science and Engineering, Basic Energy Sciences, U.S. Department of Energy, under Grant No. DE-FG02-09ER46558 (K.H.B).

References

[1] Castleman A W and Bowen K H 1996 *The Journal of Physical Chemistry* **100** 12911-44
[2] Morse M D, Geusic M E, Heath J R and Smalley R E 1985 *The Journal of Chemical Physics* **83** 2293-304
[3] de Heer W A 1993 *Reviews of Modern Physics* **65** 611-76
[4] Hashmi A S K and Hutchings G J 2006 *Angewandte Chemie International Edition* **45** 7896-936
[5] Zemski K A, Justes D R, Bell R C and Castleman A W 2001 *The Journal of Physical Chemistry A* **105** 4410-7
[6] Benten W, Nilius N, Ernst N and Freund H J 2005 *Physical Review B* **72** 045403
[7] Vossmeyer T, Katsikas L, Giersig M, Popovic I G, Diesner K, Chemseddine A, Eychmueller A and Weller H 1994 *The Journal of Physical Chemistry* **98** 7665-73

[8] Popok V N, Barke I, Campbell E E B and Meiwes-Broer K-H 2011 *Surface Science Reports* **66** 347-77
[9] Jensen P 1999 *Reviews of Modern Physics* **71** 1695-735
[10] Bardotti L, Jensen P, Hoareau A, Treilleux M, Cabaud B, Perez A and Aires F C S 1996 *Surface Science* **367** 276-92
[11] Bréchignac C, Cahuzac P, Carlier M d F, A. Masson F, Mory C, Colliex C and Yoon B 1998 *Physical Review B* **57** R2084-R7
[12] Fuchs G, Melinon P, Santos Aires F, Treilleux M, Cabaud B and Hoareau A 1991 *Physical Review B* **44** 3926-33
[13] Goldby I M, Kuipers L, von Issendorff B and Palmer R E 1996 *Applied Physics Letters* **69** 2819-21
[14] Tong X, Benz L, Kemper P, Metiu H, Bowers M T and Buratto S K 2005 *Journal of the American Chemical Society* **127** 13516-8
[15] Tournus F, Bardotti L and Dupuis V 2011 *Journal of Applied Physics* **109** 114309-4
[16] Di Vece M, Young N P, Li Z, Chen Y and Palmer R E 2006 *Small* **2** 1270-2
[17] Vandamme N, Janssens E, Vanhoutte F, Lievens P and Haesendonck C V 2003 *Journal of Physics: Condensed Matter* **15** S2983
[18] Saito Y, Murata K, Hamaguchi K, Fujita H, Kotake S, Suzuki Y, Senoo M, Hu C W, Kasuya A and Nishina Y 1998 *Journal of Cluster Science* **9** 123-30
[19] Bardotti L, Prével B, Treilleux M, Mélinon P and Perez A 2000 *Applied Surface Science* **164** 52-9
[20] Wepasnick K A, Li X, Mangler T, Noessner S, Wolke C, Grossmann M, Gantefoer G, Fairbrother D H and Bowen K H 2011 *J. Phys. Chem. C* **115** 12299-307
[21] Price S P, Tong X, Ridge C, Shapovalov V, Hu Z, Kemper P, Metiu H, Bowers M T and Buratto S K 2011 *Surface Science* **605** 972-6
[22] White J M, Bondarchuk O, Huang X, Kim J, Kay B D, Wang L S and Dohnalek Z 2006 *Angew. Chem.* **45** 4786-9
[23] Kiran B, Kandalam A K, Rallabandi R, Koirala P, Li X, Tang X, Wang Y, Fairbrother H, Gantefoer G and Bowen K 2012 *The Journal of Chemical Physics* **136** 024317-7
[24] Rao C N R and Raveau B 1998 *Transition metal oxides : structure, properties, and synthesis of ceramic oxides* (New York: Wiley-VCH)
[25] Koirala P, Kiran B, Kandalam A K, Fancher C A, de Clercq H L, Li X and Bowen K H 2011 *The Journal of Chemical Physics* **135** 134311-12
[26] Osherov A, Matmor M, Froumin N, Ashkenasy N and Golan Y 2011 *The Journal of Physical Chemistry C* **115** 16501-8
[27] Chen Z Y and Castleman J A W 1993 *The Journal of Chemical Physics* **98** 231-5
[28] Kraft J, Rattunde O, Rusu O, Häfele A and Haberland H 2002 *Surface and Coatings Technology* **158–159** 131-5
[29] Bréchignac C, Cahuzac P, Carlier F, Colliex C, Leroux J, Masson A, Yoon B and Landman U 2002 *Physical Review Letters* **88** 196103
[30] Bottcher A, Weis P, Jester S-S, Loffler D, Bihlmeier A, Klopper W and Kappes M M 2005 *Physical Chemistry Chemical Physics* **7** 2816-20
[31] Meakin P 1983 *Physical Review Letters* **51** 1119-22
[32] Röder H, Bromann K, Brune H and Kern K 1995 *Physical Review Letters* **74** 3217-20